MICROMECHANISMS OF FERRITE-PEARLITE STEELS FRACTURE UNDER CYCLIC AND IMPACT LOADING

Pavlo Maruschak[1)], Andriy Sorochak[1)], Janette Brezinova[2)], Anna Guzanova[2)], Oleh Yasniy[1)]*
[1)] *Ternopil Ivan Pul'uj National Technical University, Ruska 56, Ternopil 46001, Ukraine*
[2)] *Technical University of Košice, Department of Technology and Materials, Košice, Slovakia*

[*]*Corresponding author: e-mail: laboratory22b@gmail.com, Tel.: +380 974072696, Department of Idustrial Automation, Ternopil Ivan Pul'uj National Technical University, Ruska 56, Ternopil 46001, Ukraine*

Abstract
During operation, the railway axle is exposed to static, cyclic and dynamic loading that is accompanied by influence of corrosive environments. This causes the accumulation of structural and mechanical damages in the material, formation of corrosion and mechanical micro-defects that are potential sites of fatigue crack nucleation and growth. This requires the development of failure analysis methods that allow determining main mechanisms of ferrite-pearlite steels fracture on the micro scale level. The railway axle's material – the OSL steel – main regularities of temperature influence on fracture mechanisms in ferrite-pearlite steel type are shown. Qualitative and quantitative analysis of fracture surface of Charpy specimens tested at 20°C and -40°C was performed on micro scale level using SEM investigation.

Keywords: fracture, railway axle, dynamic loading, impact test

1   Introduction
Increase in the intensity of rail transportation leads to the increase of locomotive park usage and decrease its outage, including overhaul periods [1, 2]. Such actions require review and extending of existing approaches in particular justification of fatigue life and crack growth resistance of railway axle steel [3-5]. The solution to this problem is impossible without obtaining experimental data about influence of exploitation and temperature factors on fracture mechanisms of railway axle steel [6].

That is why considerable attention is paid to their research and obtained data are used for development of residual life assessment models. Calculation of those parameters allow evaluating probability of railway wheel-sets destruction under defined operation time and applying arrangements for durability increase of their axles [7]. A significant number of axles' defectoscopy methods are known using nondestructive inspections. Their advantage is the ability to detect surface and even internal short cracks that creates the opportunity for the axle residual life assessment, its refurbishing and restoration into the repair size.

A significant role is played by research of the effect of the exploitation defects shape influence on the axle residual life and statistical description of fatigue crack growth, the impact of the axle geometry on fatigue cracks nucleation and growth, the stress intensity factor determination at the crack tip [8, 9]. The differences in the wheel-set axle material microstructure were revealed depending on radius and influence of technological factors on homogeneous and fine-grained axle microstructure formation was analyzed, in particular blank cogging on blooming and normalization temperature [10-12].

The purpose of this work is to evaluate influence of axle steel microstructure on macro and micro mechanisms of the wheel-set axle fracture under cyclic and impact loading.

2 Research technique

The fatigue crack growth of railway wheel-set axle material – the OSL steel – was investigated on the prismatic specimens with central crack with 155x25x5 mm dimensions. Material properties are given in **Table 1**. Specimens were cut from the wheel-set axle on wheel seat zone with diameter 194 mm (**Fig. 1, a**) in the longitudinal direction on 20, 50, and 81 mm distance from its center (**Fig. 1, c**).

Tests were performed according to the ASTM E647-15 standard under uniaxial tension with stress ratio $R = -1$ and $R = 0$; maximum tensile stress on specimens $\sigma_{max} = 45...180$ MPa ($\sigma_{max}/\sigma_y = 0.12...0.48$). Loading frequency was 10 Hz; the cycle form was sinusoidal. Fatigue crack growth was investigated under room temperature on the servo-hydraulic testing rig STM-100 with the computer control system BISS 2370. During tests, control on loading process was performed by one measuring line with simultaneous information registration by six measuring lines using special BISS software. The optical system based on the metallographic microscope MBS-10 was used for measuring crack length.

Table 1 Mechanical properties of the OSL steel

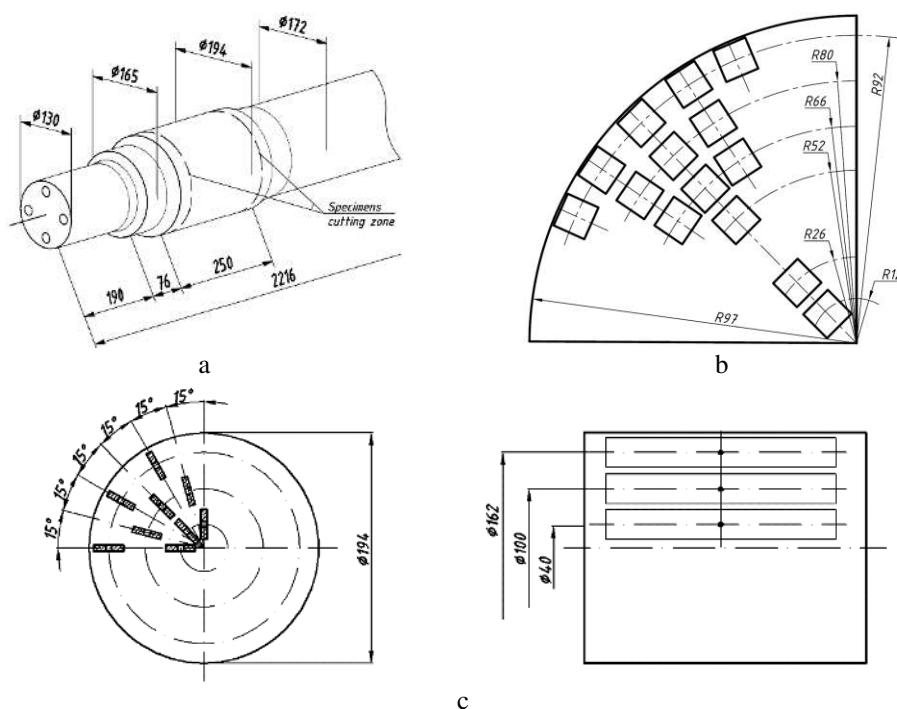| Ultimate tensile stress, σ_u, MPa	Tensile yield stress, σ_y, MPa	Elongation, ε, %	Lateral contraction, ψ, %
730	382	13,5	40

Fig. 1 Specimens cutting scheme: cutting zone location (a), Charpy (b) and fatigue crack growth (c) specimens cutting scheme

The temperature influence on the impact toughness was determined on Charpy specimens with 10x10x55 mm dimensions and V-notch with 0.25 ± 0.025 mm radius. Specimens were cut from the axle wheel seat zone of 194 mm diameter on different distance from its center (**Fig. 1, b**). The tests were performed on the RKP-300 impact testing machine with the impact energy of 300 J equipped with the loading diagram recording system in "impact force versus time" and "impact force versus displacement" coordinates according to the ISO 14556:2015 standard. Two test series were performed under +20ºC and -40ºC temperatures.

Test specimens were cut out from railway axle using milling machine in low cutting speed mode with mandatory use of liquid lubricant-coolant and further grind process. Specimens for fatigue crack growth test were additionally manually polished to surface roughness value *Ra* 0,32 for working area.

3   Steel properties and grain structure

It is well known that macroscopic material behavior is governed by its microstructure. In general, carbon steels are characterized by the precipitation of cementite, which is iron carbide, into various forms. A typical microstructure of ferrite-pearlite steel is composed of several ferrite crystal grains and pearlite blocks. A pearlite block contains some pearlite colonies characterized by the lamellar structures of ferrite and cementite phases. Such hierarchical heterogeneity is the dominant factor of its strength and deformation characteristic [13, 14].

Locomotive wheel-set axles under operation experience vertical and horizontal loads and torsion as well. Severe conditions demand for increased requirements to the material of axles, especially to cyclic durability and crack resistance. Domestic wheel-set axles are made of the OSL steel (Russian standard GOST 4728-96) with chemical composition of: C 0.40–0.48; Mn 0.55–0.85; Si 0.15–0.35; P 0.04; S 0.045; Cr 0.3; Ni 0.3; Cu 0.25%.

Fracture surfaces of different specimens cut from the railway axle were investigated on the SELMI REM-106I raster electron microscope in the secondary electrons mode with the following parameters: cathode voltage – 20–30 kV, current – 160–200 μA, focal distance – 9-15 mm. Specialized KAPPA ImageBase software was used for the quantitative analysis of the obtained images.

The microstructure of the OSL steel is presented on **Fig. 2**. The steel is referred to ferrite-pearlite type one. Electron-microscopy studies revealed the presence of structurally free ferrite, as well as pearlite colonies located in different parts of ferrite grains (Fig. 2, a). It is found by the analysis of SEM-micrographs that the ferrite grains occupy about 30% of the tested area in the specimen under investigation. Their average size makes about 10 μm, (**Fig. 2, b**).
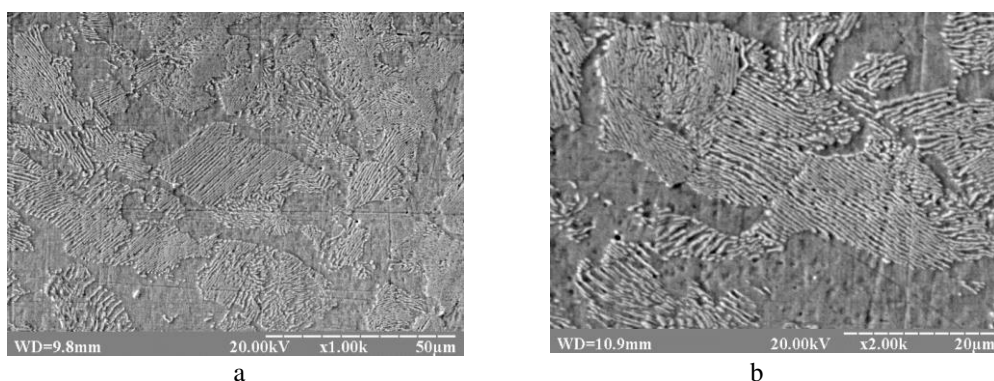

a   b

Fig. 2 Microstructure of the OSL steel (a), ferrite and pearlite grains (b)

The average size of pearlite colonies is 15 μm, the distance between the cementite plates is 0.2 μm at the average. By dispersion of plate cementite, the structure can be described as sorbite. This type of structure is characterized by high strength and toughness with high hardness, which improves the performance of railway transport axles [15-17].

Fig. 3 shows a histogram of the OSL steel grain sizes obtained from microscopy analysis. The particle distribution histogram was obtained counting 574 grains from the micrograph. The solid line corresponds to the log-normal distribution fit and gives us an average grain size of 11.50 μm and a standard deviation $\sigma = 6.53$.
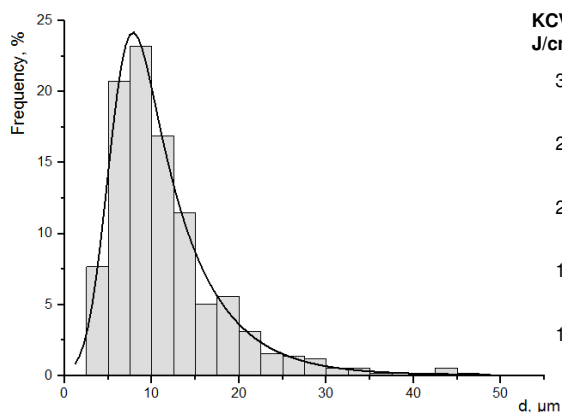

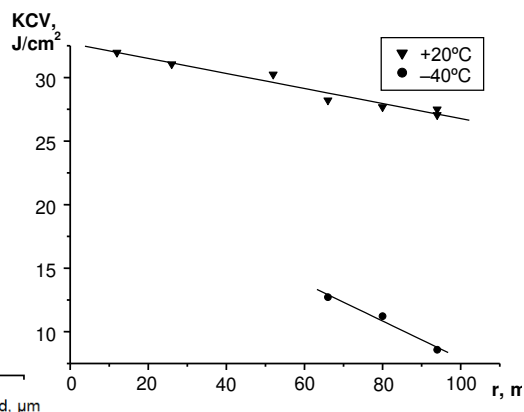**Fig. 3** Grain size histogram of the OSL steel

Fig. 4 Dependence of impact toughness on the undercut radius of specimens [18]

4   Micromechanisms of fracture under impact loading

Obtained results showing inversely proportional dependency of the impact toughness on the specimens undercut radius from the locomotive wheel-set axle (**Fig. 4**). Particularly, with the increase of undercut radius from 12 mm to 94 mm the impact toughness decreases to 15.6 % at temperature +20ºC, and with the change of undercut radius from 66 mm to 94 mm at -40ºC this parameter decreases to 32.5 %. The reasons of this phenomenon can be in the technology of railway axles manufacturing, during which an axle is subjected to the strengthening treatment by a roller on a full length for the increase of high-cycle fatigue resistance. The decrease of test temperature from +20 to -40ºC decreases significantly the impact toughness and portion of ductile fracture. For the near-subsurface layers of axle impact toughness decreases by more than 3 times [18].

Charpy specimens were investigated under +20 and -40°C temperature and their fracture surface was investigated using SEM. Processes of deformation and fracture were divided into stages of initiation and propagation of the crack in Charpy specimens.

Crack initiation

Test temperature 20°C. The fracture surface has a fibrous view, which testifies to ductile failure (**Fig. 5, a**). The width of the crack initiation zone is 250…270 μm. The consecutive sections of the dimple ductile-brittle intragranular failure and sections of quasi-spalling represent fracture surface of the OSL steel in the crack initiation zone. The dimples have a circular shape and a size

of 5–10 μm, they are located on the surface of the ductile separation sections of a greater scale. Circular dimples have the elongated shape on individual sections. Ductile ridges formed due to plastic deformation of pores enclose the dimples [19].

Test temperature −40°C. The fracture is brittle and has multiple dimples of size 7–10 μm (**Fig. 5, c**). The dimples are not deep, approximately identical in size, have sharp ridges located within one area. Flat structureless sections are found between the dimples. We can presume that the number of dimples is proportional to the number of pores; moreover, a low dispersion of dimple sizes testifies to a significant "self-organization" and synchronism of their growth [20].
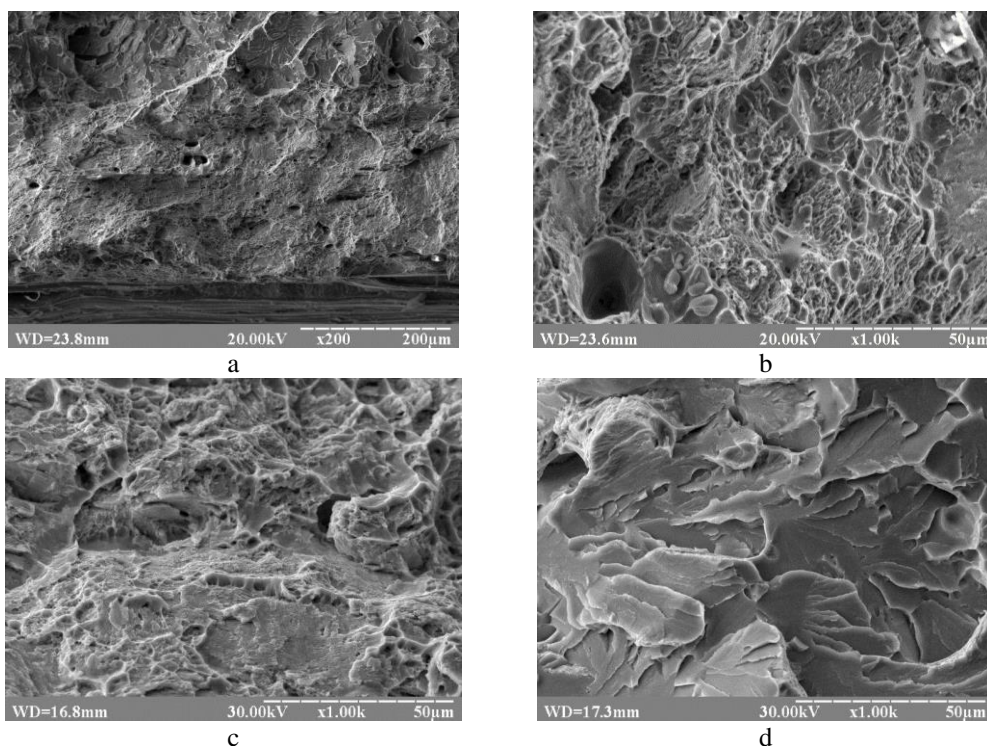

Fig. 5 SEM micrographs of the impact fracture surface of the OSL steel at 20°C (a-c) and at −40°C (d)

Crack propagation.

Test temperature 20°C. Fracture took place by the ductile-brittle mechanism. The main elements of the fracture surface are the sections of microspalling and the sections of the micro-dimple relief with the formation of "steps" and local plastically deformed sections. Plastic deformation occurred on the net cross section of specimens. Fracture took place by the mechanism of mixed (brittle-ductile) fracture (**Fig. 5, b**).

Within the crack propagation zone, the surface is formed by the facets of brittle spalling and facets with the V-ribbed pattern. Facets decorated with parallel strips characterize the intragranular failure of pearlite grains.

Test temperature −40°C. Brittle fracture occurred without a distortion of the specimen cross section. The presence of the facets of spalling, whose sizes are commensurable with the grain size, testifies to the predominant mechanism of brittle fracture. The process of fracture took place

within several areas with the developed fracture surface, on which the disoriented scars and ridges were observed (**Fig. 5, d**).

We can presume that a significant influence on the fracture mechanism was caused by the structural-mechanical defects. This is evidenced by the location of microspalling facets. Localized cracks are detected between microfacets that have a corrugated surface.

5　Marco- and micromechanisms of fracture under cyclic loading

Kinetic diagrams of fatigue crack growth in OSL steel and their approximation by Paris law under $R = 0$ and $R = -1$ are depicted on **Fig. 6**, where $\Delta K = K_{max} - K_{min}$ − stress intensity factor (SIF) range, K_{max} − maximal SIF, K_{min} − minimal SIF in loading cycle.

Crack growth rate on the middle-amplitude zone under $R = 0$ is almost independent from the specimen cutting radius but the threshold SIF range ΔK_{th} of the specimen undercut from the near-surface layer is greater than ΔK_{th} of the specimen undercut from the middle axle layer. As for kinetic diagram of fatigue fracture for $R = 0$, specimen cutting radius has minor influence on the crack growth rate on the middle-amplitude zone under $R = -1$. However, unlike $R = 0$, the threshold SIF range ΔK_{th} of the specimen undercut from the middle axle layer is greater than ΔK_{th} of the near-surface layer material.
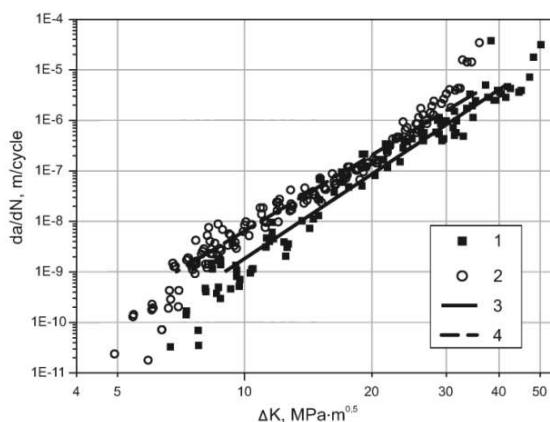

Fig. 6　Kinetic diagram of fatigue crack growth rate of the OSL steel under $R=0$ (1) and $R=-1$ (2) and its approximation by Paris law for $R=0$ (3) and $R=-1$ (4) [7]

Load ratio R = 0. The fracture surface is formed by the ductile-brittle mechanism and consists of numerous terraces decorated with the fragmentarily located series of striations (**Fig. 7, a, b**). Disoriented relief formations are noticeable on the fracture surface at low crack growth rate zone ($da/dN < 10^{-9}$ m/cycle). The facets of the intragranular failure are covered with typical fatigue striations with quite a large step of 1 μm, which alternate with the split pearlite grains, whose failure took place by means of spalling across the crack of the cementite plate. However, even within individual facets, the orientation of striations was not permanent [21, 22].

The specimen surface at medium crack growth rate zone (10^{-9} m/cycle $\leq da/dN \leq 10^{-6}$ m/cycle) is fragmented heavily, therefore, we can speak only about the macrodirection of crack propagation. The crack front moved from one octahedral area to another, forming terraces and steps, due to which the terrace acquired a curvilinear trajectory (**Fig. 7, c**). It should be noted that due to a complex stress state in the cyclic plastic zone in front of the crack tip, the direction of the lines of

fatigue striations differ significantly in the neighboring structural elements (**Fig. 7, c**), since the fatigue crack propagates locally in the direction with the minimal fracture energy [23-25].
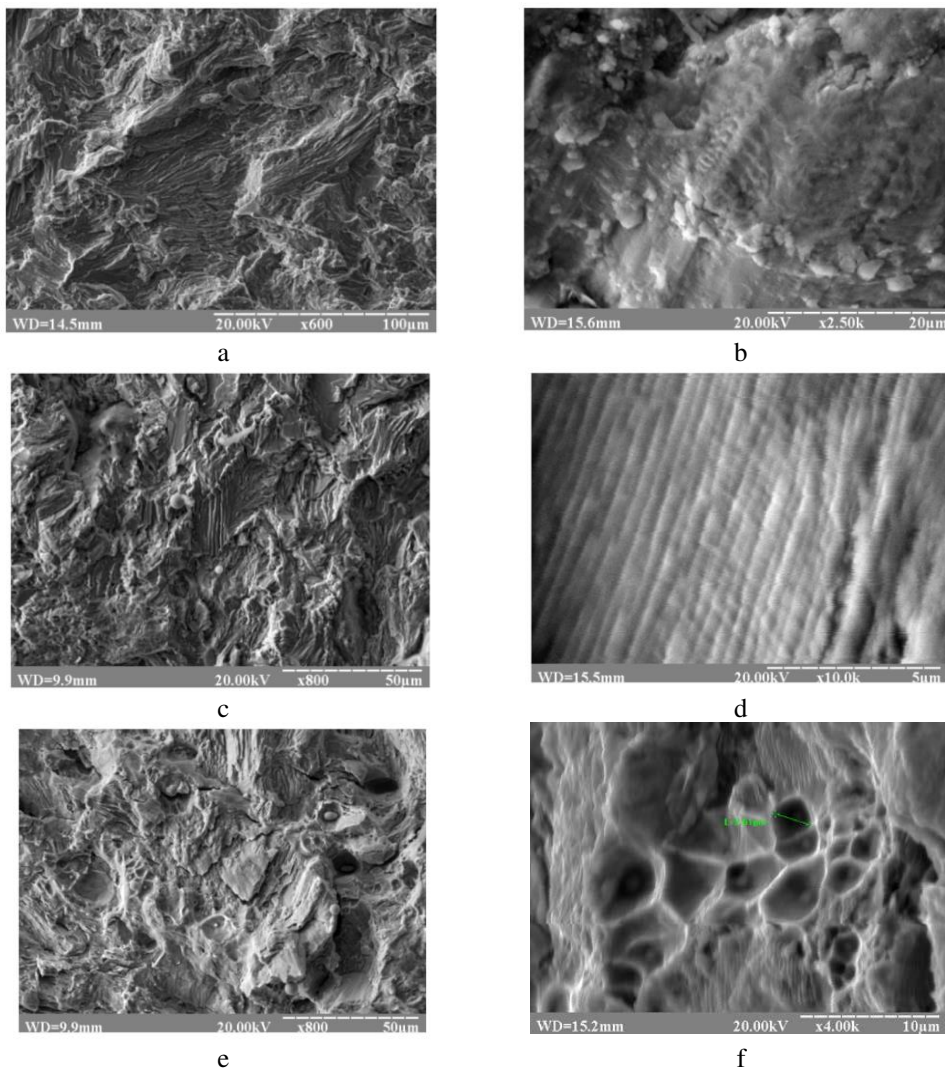

Fig. 7   SEM micrographs of the fatigue crack growth in the OSL steel in case of loading cycle stress ratio $R = 0$

At the same time, terraces geometry indicates that during crack propagation they created the local relaxation sections. This causes a decrease in the microrate of crack propagation (step of fatigue striations) on individual sections of the crack front, which was observed on the fracture surface. The fatigue crack growth within the high rate zone ($da/dN > 10^{-6}$ m/cycle) determined the transition of deformation mechanisms to the macroscale level and an increase in the FCR rate. An increase in the crack length had practically no effect on the crack propagation mechanism, only the share of ductile separation was increasing, and the striation mechanism disappeared gradually (**Fig. 7, d**). At high propagation rates and within the zone of static rupture of the specimen material, a typical dimple failure was observed, and some inclusions of the circular and oblong shape were

noticeable at the bottom of individual dimples (**Fig. 7, e**). The crack growth mechanisms acquire ductile character, which preconditions the increased strain localization and the effect of rotational plasticity. An increase in the level of plastic deformation causes the localization of plastic strains in the vicinity of the microstructure elements: inclusions, subgrain boundaries, microfailure and separation of coherent links between inclusions and the matrix, which explains the formation of the local zones of dimple separation. Crack propagation is accompanied by the activation of secondary cracking and branching of the main crack.

With an increase in the crack length, the influence of inclusions and disperse particles on the fatigue crack propagation mechanisms increases. Large separation dimples, which were formed due to separation of inclusions from the matrix, are noticeable on the fracture surface (**Fig. 7, f**). Significant strains along the body and within the grains facilitate the development of the plastic zone at the crack tip, thus speeding up failure processes and causing the formation of individual microcracks, which then coalesce with the main crack.

Load ratio R = -1. Failure of the material took place by the mechanisms similar to stress ratio $R = 0$. The crack propagated in the non-uniform manner, fracture had a ductile-brittle character (**Fig. 8, a**). It should be noted that the front of the fatigue crack penetration at the low crack growth rate zone is fragmented heavily, it is covered with terraces and "steps". This indicates the activation of shear processes within the pearlite grains [23-25].

The fracture surface at the medium crack growth rate zone is formed by the "corrugated" relief (**Fig. 8, b**), which is located at different angles relative to the crack propagation direction, the striations are located on the surfaces of terraces. The crack front propagated in the non-uniform manner, which indicates strain localization within certain sections of the materials.
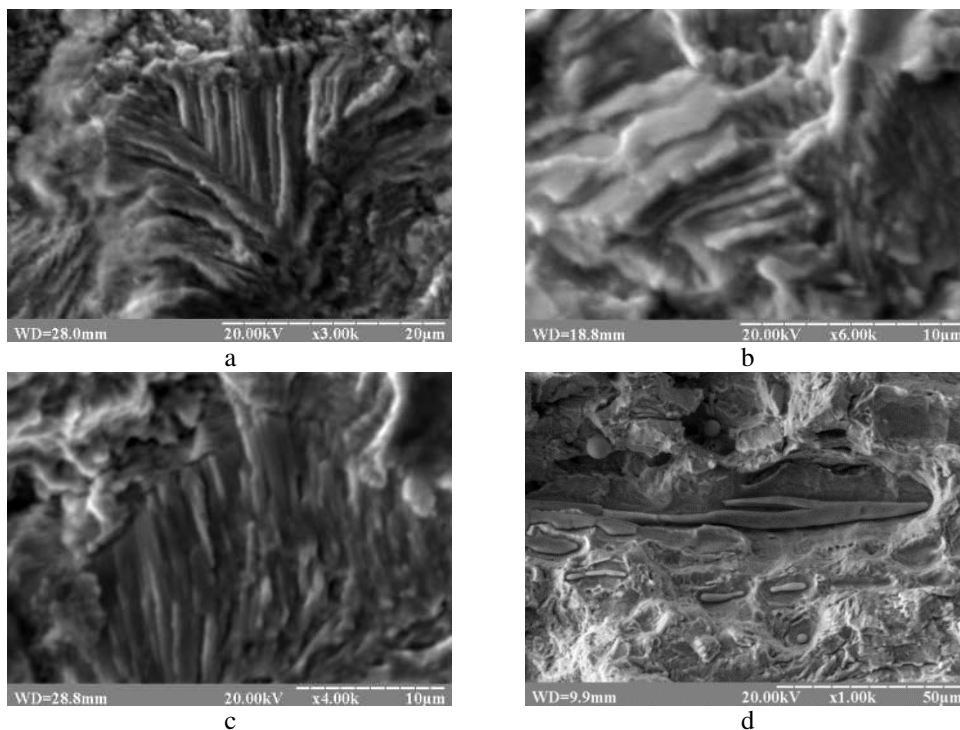

a   b

c   d

Fig. 8 SEM micrographs of the fatigue crack growth in the OSL steel in case of loading cycle stress ratio $R = -1$

Well-developed sections of crushing of the fracture surface were observed (**Fig. 8, c**), which indicates the crack closure. However, like in the previous case, the crack propagated by the striation mechanism, which then changed into the mixed one and had a ductile character within the pre-failure zone. There are visible dimple fractures at the surface formed by the inclusions cleavages from the matrix (**Fig. 8, d**).

Observed at the macrolevel decrease in the fatigue crack propagation rate at the loading cycle stress ratio $R = -1$ compared to $R = 0$ is caused by the crack branching processes in the pearlite grains and local blunting of the crack tip in the ferrite component (section I). Therefore, an increase in the active loading time during the specimen loading did not ensure the accumulation of structural damage; however, it contributed to the activation of the relaxation processes in the material and, correspondingly, a decrease in the fatigue crack growth rate. It should be noted that the size of microbranching was less than that of the ferrite grains, which hampered the crack propagation during its growth through the pearlite grains. Moreover, the fragmentation and milling of the cementite plates took place in the pearlite grains.

However, with an increase in the size of the pearlite zone, greater volumes of the material become involved in the deformation process, which preconditions an increase in the intensity of the structural defect accumulation in the grain conglomerates (section III). In addition, the crack propagation mechanisms at different asymmetries become more similar, which is depicted on the kinetic curve [7].

The micromechanisms of the OSL steel fracture under fatigue and impact loading are summarized in the **Table 2**.

Table 2 Fracture mechanisms of the OSL steel

Specimen loading	Fracture mechanisms	Fracture surface characteristic
Dynamic	Mixed (brittle–ductile) fracture at 20°C; Brittle shear at -40°C	Localized strains of microsections of the material, the formation of microcracks around the particles of the secondary phases and fragmentation of the microfracture process. The presence of the facets of spalling, whose sizes are commensurable with the grain size
Cyclic	Striation mechanism; Facets of spalling; Facets of failure of pearlite grains; Ductile separation dimples	Numerous terraces decorated with the fragmentarily located series of striations, facets of the intragranular failure. With stress intensity factor increase ductile separation increasing and the striation mechanism disappearing gradually. Crack propagation is accompanied by the activation of secondary cracking and branching of the main crack.

Conclusions

The influence of temperature and undercut radius of specimens on impact toughness and micromechanisms of fracture of the material of railway axle is investigated. SEM analysis of fracture surfaces of specimens shows the presence of successive areas of dimple ductile fracture and areas of cleavage. With the decrease of test temperature to –40 ºC the portion of ductile fracture is considerably reduced.

The influence of the pearlite colonies on the fatigue crack propagation kinetics was observed, which was depicted in the presence of the fatigue and ductile-brittle crack propagation sections on the surface. In our opinion, the pearlite colonies, which are located on the trajectory of the fatigue crack tip, cause the relaxation effects. However, an increase in the stress intensity factor causes an increase in the share of the ductile propagation of the crack, in particular, the dimple component, which causes a decrease in the size of the separation facets and the appearance of the ductile separation dimples.

References
[1] H. Alihosseini, K. Dehghani: Journal of Failure Analysis and Prevention, Vol. 10, 2010, p. 233-239, DOI:10.1007/s11668-010-9340-0
[2] M. Bayraktar, N. Tahrali, R. Guclu: Journal of Mechanical Science and Technology, Vol. 24, 2010, p. 671-679, DOI:10.1007/s12206-009-1219-1
[3] Y.X. Zhao, B. Yang, M.F. Feng, H. Wang: Int. J. Fatigue, Vol. 31, 2009, p. 1550-1558, DOI:10.1016/j.ijfatigue.2009.04.016
[4] S. Cervello: Fatigue properties of railway axles: Int. J. Fatigue, Vol. 86, 2016, p. 2-12, DOI:10.1016/j.ijfatigue.2015.11.028
[5] S. Beretta, M. Carboni, G. Fiore, A. La Conte: Int. J. Fatigue, Vol. 32, 2010, p. 952-961, DOI:10.1016/j.ijfatigue.2009.08.003
[6] A.P. Sorochak Fracture toughness and residual life of wheelset axles considering structural and mechanical heterogeneity, Dissertation for Candidate of Science degree in Engineering, Ternopil Ivan Pul'uj National Technical University, Ternopil, 2015
[7] O. Yasniy, Y. Lapusta, Y. Pyndus, A. Sorochak, V. Yasniy: Int. J. Fatigue, Vol. 50, 2013, p. 40-46, DOI:10.1016/j.ijfatigue.2012.04.008
[8] D.S. Hoddinott: Proceedings of the Institution of Mechanical Engineers, Part F: Journal of Rail and Rapid Transit, Vol. 218, 2004, p. 283-292, DOI:10.1243/0954409043125897
[9] A. Sorochak, P. Maruschak, O. Prentkovskis: Transport and Telecommunication, Vol. 16, 2015, p. 158-166, DOI:10.1515/ttj-2015-0015
[10] J.M. Hyzak, I.M. Bernstein: Metallurgical Transactions A, Vol. 7, 1976, p. 1217-1224, DOI:10.1007/BF02656606
[11] M. Zhang, H. Gu: Journal of University of Science and Technology Beijing, Vol. 15, 2008, p. 125-131, DOI:10.1016/S1005-8850(08)60025-0
[12] A. Gianni, A. Ghidini, T. Karlsson, A. Ekberg: Proceedings of the Institution of Mechanical Engineers, Part F: Journal of Rail and Rapid Transit, Vol. 223, 2009, p. 163-171, DOI:10.1243/09544097JRRT217
[13] I. Watanabe, D. Setoyama, N. Nagasako, N. Iwata, K. Nakanishi: Int. J. Numer. Meth. Engng. Vol. 89, 2012, p. 829-845, DOI:10.1002/nme.3264
[14] P. Maruschak, A. Sorochak, S. Panin: Applied Mechanics and Materials, Vol. 770, 2015, p. 209-215, DOI:10.4028/www.scientific.net/AMM.770.209
[15] Y. Huo, J. Lin, Q. Bai, B. Wang, X. Tang, H. Ji: Journal of Materials Processing Technology, Vol. 239, 2017, p. 359-369, DOI:10.1016/j.jmatprotec.2016.09.001
[16] Y. Huo, Q. Bai, B. Wang, J. Lin, J. Zhou: Journal of Materials Processing Technology, Vol. 223, 2015, p. 274-283, DOI:10.1016/j.jmatprotec.2015.04.011
[17] P.O. Maruschak, S.V. Panin, F. Stachowicz, I.M. Danyliuk, I.V. Vlasov, R.T. Bishchak: Acta Mechanica, Vol. 227, 2016, p. 151-157, DOI:10.1007/s00707-015-1420-5

[18] O. Yasniy, T. Vuherer, Y. Pyndus, A. Sorochak, I. Samardžić: Technical Gazette, Vol. 18, 2011, p. 87-90

[19] O.P. Modi, M.N. Desmukh, D.P. Mondal, A.K. Jha, A.H. Yegneswaran, H.K. Khaira: Materials Characterization, Vol. 46, 2001, p. 347-352, DOI:10.1016/S1044-5803(00)00113-3

[20] P. Maruschak, D. Baran, V. Gliha: Medžiagotyra, Vol. 19, 2013, p. 29-33, DOI:10.5755/j01.ms.19.1.3821

[21] P.O. Maruschak, D.Ya. Baran, A.P. Sorochak, R.T. Bishchak, V.P. Yasnii: Strength of Materials, Vol. 44, 2012, p. 410-418, DOI:10.1007/s11223-012-9395-0

[22] A.A. Shanyavskiy, L.M. Burchenkova: Int. J. Fatigue, Vol. 50, 2013, p.47-56, DOI:10.1016/j.ijfatigue.2012.04.006

[23] A.A. Shanyavskiy, M.A. Artamonov: Int. J. of Fracture, Vol. 128, 2004, p. 309-314, DOI:10.1023/B:FRAC.0000040994.96074.bf

[24] J. Wawszczak, K.J. Kurzydłowski: Materials Characterization, Vol. 60, p. 1180-1184, DOI:10.1016/j.matchar.2009.02.014

[25] I. Černý, V. Linhart: Key Engineering Materials, Vols. 592-593, 2014, p. 631-634, DOI:10.4028/www.scientific.net/KEM.592-593.631